

Micro and nano-patterned silk substrates for antifouling applications

Gabriele Tullii, Stefano Donini, Caterina Bossio, Francesco Lodola, Mariacecilia Pasini, Emilio Parisini, Francesco Galeotti, and Maria Rosa Antognazza

ACS Appl. Mater. Interfaces, **Just Accepted Manuscript** • DOI: 10.1021/acsami.9b18187 • Publication Date (Web): 09 Jan 2020

Downloaded from pubs.acs.org on January 13, 2020

Just Accepted

“Just Accepted” manuscripts have been peer-reviewed and accepted for publication. They are posted online prior to technical editing, formatting for publication and author proofing. The American Chemical Society provides “Just Accepted” as a service to the research community to expedite the dissemination of scientific material as soon as possible after acceptance. “Just Accepted” manuscripts appear in full in PDF format accompanied by an HTML abstract. “Just Accepted” manuscripts have been fully peer reviewed, but should not be considered the official version of record. They are citable by the Digital Object Identifier (DOI®). “Just Accepted” is an optional service offered to authors. Therefore, the “Just Accepted” Web site may not include all articles that will be published in the journal. After a manuscript is technically edited and formatted, it will be removed from the “Just Accepted” Web site and published as an ASAP article. Note that technical editing may introduce minor changes to the manuscript text and/or graphics which could affect content, and all legal disclaimers and ethical guidelines that apply to the journal pertain. ACS cannot be held responsible for errors or consequences arising from the use of information contained in these “Just Accepted” manuscripts.

Micro and nano-patterned silk substrates for antifouling applications

G. Tullii^{1,2,3}, S. Donini¹, C. Bossio¹, F. Lodola¹, M. Pasini³, E. Parisini¹, F. Galeotti³ and M. R. Antognazza^{1,}*

¹Center for Nano Science and Technology@PoliMi, Istituto Italiano di Tecnologia, via Pascoli 70/3, 20133, Milano, Italy.

²Department of Physics, Politecnico di Milano, Piazza L. Da Vinci 32, 20133, Milano, Italy.

³Istituto di Scienze e Tecnologie Chimiche "Giulio Natta", Consiglio Nazionale delle Ricerche (SCITEC-CNR),
Via Alfonso Corti 12, 20133 Milano, Italy

Keywords: silk fibroin; antifouling; conjugated polymer; microstructured surface; E. coli; breath figures;
biofilm inhibition

ABSTRACT

A major problem of current biomedical implants is due to bacterial colonization and subsequent biofilm formation, which seriously affects their functioning and can lead to serious post-surgical complications. Intensive efforts have been directed towards the development of novel technologies that can prevent bacterial colonization while requiring minimal antibiotics doses. To this end, biocompatible materials with intrinsic antifouling capabilities are in high demand. Silk fibroin, widely employed in biotechnology, represents an interesting candidate.

Here, we employ a soft-lithography approach to realize micro- and nano-structured silk fibroin substrates, with different geometries. We show that patterned silk film substrates support mammal cells (HEK-293) adhesion and proliferation, and at the same time they intrinsically display remarkable antifouling properties. We employ *Escherichia coli* as representative gram-negative bacteria and we observe a up to 66% decrease in the number of bacteria that adhere to patterned silk surfaces as compared to control, flat silk samples. The mechanism leading to the inhibition of biofilm formation critically depends on the microstructures geometry, involving both a steric and a hydrophobic effect. We also couple silk fibroin patterned films to a biocompatible, optically-responsive organic semiconductor, and we verify that the antifouling properties are very well preserved.

The technology described here is of interest for the next-generation of biomedical implants, involving the use of materials with enhanced antibacterial capability, easily processable, highly biocompatible and promptly available for coupling with photoimaging and photodetection techniques.

1. Introduction

In recent years, silk fibroin has been eliciting an ever increasing interest in the biotechnology field. Several applications have been reported, spanning from tissue engineering^{1,2} to regenerative medicine,³⁻⁹ from drug delivery¹⁰⁻¹² to bio-photonics,¹³⁻²⁰ from implantable devices²¹⁻²⁵ up to the last frontiers in bioengineering, the realization of bio-degradable, bio-resorbable and edible electronic devices.²⁶⁻³⁰ The main reason behind such a success story relies on the peculiar advantages offered by silk, in terms of outstanding mechanical properties, chemical-physical versatility due to its polymorphic character, thermal and environmental stability, suitability to several processing techniques (easily allowing for covering dimensions from the nano- to the macro-scale), endless opportunities of functionalization with biomolecules and drugs, and excellent cytocompatibility. Overall, silk is widely recognized as a highly promising material platform, with global impact in the biomedical, biophotonics and bioelectronics fields.³¹

The development of silk-based materials for implantable biotechnological devices has fostered the investigation of the benefits of silk functionalization with antimicrobial agents.³²⁻³⁵ In fact, the main, hardly addressable risk leading to failure of medical implants is represented by microbial contamination, which causes device-associated severe infections.³⁶ Bacteria preferentially adhere and proliferate on the implant surface, producing a biofilm, i.e. a layer of aggregated bacteria embedded into a matrix composed of extracellular polymeric substances such as proteins, DNA and polysaccharides.³⁷ The presence of the biofilm confers to the microorganisms a much higher resistance than the unattached bacteria, requiring 500–5000 times higher doses of antibiotics.^{37,38} Some literature reports have addressed this problem by taking advantage of the chemical versatility of silk and by functionalizing the silk-based implant with antimicrobial agents. Unfortunately, this approach, albeit capable of substantially reducing bacterial contamination, has a serious drawback, since the extensive use of antibiotics inevitably leads to an enhanced bacterial resistance towards the common antibiotic agents, thus establishing a vicious circle.

A solution consists in the hindering of the formation of the biofilm (antifouling) by properly engineering implanted materials and devices.³⁹ It has been widely reported that microbial adhesion can be efficiently limited by modifying the material surface properties through the control of physical-chemical parameters

1
2
3 1 such as steric hindrance, hydrophobicity, Van der Waals forces or electrostatic interactions.^{40–44} Nature offers
4
5 2 multiple examples of fouling control strategies employed by animal and plants, which involve different
6
7 3 physical-chemical approaches. The latter are often associated to the presence of micro/nano-patterned
8
9 4 surface topographies characterized by various diameters, widths, lengths, heights, and pitches.^{40,45–47}
10
11 5 Laboratory research has been oriented to the mimic of these morphologies, finding that the tuning of the
12
13 6 micro/nano-structure parameters may prevent surface colonization by specific microorganisms.^{45,46} Many
14
15 7 organic biomaterials have been tested, including, among others, poly(dimethylsiloxane), polyurethane,
16
17 8 cellulose, poly(ethylene glycol) and thiophene-based conducting polymers.^{45,47,48} Surprisingly, the endless
18
19 9 possibilities offered by silk manufacturing and processing techniques just started to gain attention. In a very
20
21 10 recent work by Chu and colleagues, the nanostructuring of silk substrates was first reported for orthopedic
22
23 11 implants.⁴⁹ Moreover, it has been widely reported that proper modulation of the surface topography may
24
25 12 strongly affect proliferation, migration and stem cells differentiation processes.⁵⁰ This may open interesting
26
27 13 perspectives towards the realization of a double-functional device, endowing antifouling properties and
28
29 14 mechanical cues for specific cell-substrate interaction and metabolism modulation.

30
31
32 15 In this work, we report the preparation of micro and nano-patterned silk surface topographies and the
33
34 16 quantification of the adhesion grade of GFP-encoded *Escherichia coli* (*E. coli*) bacteria by means of
35
36 17 fluorescence microscopy imaging. We observe a reduction in bacterial adhesion on structured surfaces up
37
38 18 to 66% as compared with unpatterned substrates. Importantly, this is not accompanied by alteration in the
39
40 19 cytocompatibility of the patterned silk substrate, as evaluated by viability assays with mammal cell model
41
42 20 cultures. In view of possible applications in the bio-photonics field, we also couple silk-based substrates to
43
44 21 light-sensitive organic semiconducting polymer with distinct optoelectronics properties. We verify that the
45
46 22 coating with the polymer does not hinder the antifouling effect shown by the patterned silk substrates. Our
47
48 23 work offers interesting perspectives in the realization of novel silk-based biocompatible devices, endowed
49
50 24 with both antifouling and photonics functionalities.

2. Experimental

2.1 Materials and silk substrates fabrication

Regio-regular poly(3-hexylthiophene-2,5-diyl) (rr-P3HT) (purity 99.995%, molecular weight 15000 - 45000), o-dichlorobenzene, Dulbecco's Modified Eagles Medium (DMEM), Trypsin-EDTA, Penicillin, phosphate buffer saline (PBS) tablets, streptomycin, fibronectin (from bovine plasma), 3-(4,5-dimethylthiazol-2-yl)-2,5-diphenyltetrazolium bromide (MTT), LiBr, Ampicillin, EtOH were purchased from Sigma Aldrich. PDMS elastomer (Sylgard 184) was purchased from Dow Corning. Fetal Bovine Serum (FBS) was purchased from Euroclone. All chemicals were used without any further purification.

For the preparation of silk fibroin films, *Bombyx mori* degummed silk fibers (2 g) were dissolved in a LiBr solution (9.3 M, 10 mL) at 60 °C for 90 min obtaining a 20% (w/v) solution. A dialysis tubing (molecular weight cutoff of 12 000 Da) was used for dialyzing the solution in water for 48 h at room temperature to remove the LiBr salt. The aggregates formed during dialysis were removed by centrifugation (4000 rpm, 25 min). After these steps, the aqueous silk solution concentration was approximately 6% (w/v), as determined by a gravimetric analysis performed on the dried sample. Silk solution was then casted on both flat and patterned PDMS master mold and dried in fume hood under gentle aspiration for 24 h, following the procedure described in ref ⁵¹. The patterned PDMS films were obtained by replica molding of the polycarbonate layer of a CD-ROM (to obtain the master for the nano stripes) and of honeycomb structured layers prepared by breath figure templating technique (to obtain the masters for the micro wells). The polymeric materials used and conditions of the breath figure process were defined in order to obtain two different kinds of microporous templates, with larger (~5 μm) and smaller (1-2 μm) microcavities, as described in ref ⁵² and ref ⁵³, respectively. Once solidified, the fibroin films were subjected to a water vapor annealing by placing them in a desiccator together with a water reservoir for 12 hours. This process increases the crystallinity of the silk-based material and makes it insoluble in water.⁵⁴ Then, the dry fibroin films were softened by 2 min immersion in distilled water and carefully detached from the PDMS master.

For the preparation of polymer-coated silk substrates, fibroin silk films were anchored on glass slide using adhesive tape and air-dried for one night. rr-P3HT was dissolved in o-dichlorobenzene (5 g l⁻¹) and stirred for

1
2
3 1 one night at 50 °C. rr-P3HT solution was then deposited on dry silk substrates by spin coating (speed 1500
4
5 2 rpm, acceleration 1600 rpm s⁻¹) and the obtained samples were left in vacuum for 40 minutes before use.
6
7
8 3

4 **2.2 Substrates characterization**

5 Scanning electron microscopy (SEM) micrographs were acquired using a TESCAN MIRA III scanning electron
6
7 microscope (operating voltage 4kV, working distance 19 mm, stage tilt angle 30°). Prior to SEM images
8
9 acquisition, silk substrates were attached to glass slides using adhesive tape, air-dried and covered by a thin
10
11 gold layer (thickness 6 nm, 1.5 Cr adhesion layer) using a metal evaporator. The atomic force microscopy
12
13 (AFM) images were acquired using NT-MDT NTEGRA apparatus in tapping mode under ambient conditions.
14
15 For water contact angle measurements, silk-based samples were attached to glass slides using adhesive tape
16
17 and air-dried overnight. Then, photographs of 5 µl water droplets deposited on the different substrates were
18
19 taken using an optical contact angle measuring and contour analysis system (DataPhysics OCA 15EC). The
20
21 calculation of the static water contact angle was carried out using the SCA 20 software (DataPhysics),
22
23 according to the sessile drop method.
24
25
26
27
28
29
30
31
32
33

34 **2.3 Cells cultures preparation and viability assay**

35
36 Silk substrates were sterilized by immersion in EtOH 70% for 3 hours and washed 3 times with mQ-H₂O.
37
38 Then, a layer of fibronectin (2 µg ml⁻¹ in PBS buffer solution) was deposited on the samples surface and
39
40 incubated for 1 hour at 37 °C, in order to promote cellular adhesion. Excess fibronectin was then removed
41
42 by rinsing with PBS prior to cell plating. HEK-293 cells were cultured in cell culture flasks containing
43
44 Dulbecco's modified Eagle's medium (DMEM) with 10% Fetal Bovine Serum (FBS), 100 µg l⁻¹ Penicillin and
45
46 100 µg ml⁻¹ Streptomycin. Culture flasks were maintained in a humidified incubator (Forma series II water
47
48 jacketed CO₂ incubator, Thermofisher) at 37 °C with 5% CO₂. When at confluence, HEK-293 cells were
49
50 enzymatically dispersed using trypsin-EDTA and then plated on the different samples at a concentration of
51
52 20000 cells cm⁻² and maintained in the incubator at 37 °C with 5% CO₂. Cells proliferation was assessed after
53
54 24, 48, 72 and 96 hours *in vitro* by performing the MTT assay. For each time point, the growing medium was
55
56 replaced with RPMI medium without phenol red containing 0.5 mg ml⁻¹ of MTT and the samples were
57
58
59
60

maintained in the dark at 37 °C for 3 h. Then, the medium was removed and the samples were air-dried at room temperature. Dry samples were subsequently immersed in 200 μ l of ethanol in order to dissolve the formazan salt produced by cells through reduction of MTT. The proliferation cell rate was calculated as the difference in absorbance at 560 nm and 690 nm. Statistical significance was determined by the one-way ANOVA Dunnett's post-hoc test.

2.4 Bacterial cultures and adhesion evaluation

The gene encoding eGFP was PCR amplified from a pDONR-P2R-P3 vector carrying the eGFP coding sequence, and cloned into a pET23a(+) by conventional methods using NdeI and XhoI restriction sites (Table 1). The resulting construct (pET23a(+)-eGFP) was sequence verified and transformed into *E. coli* Rosetta (DE3) competent cells (Invitrogen).

Table 1. Primer sequence (5'-3') used in this study.

| Primer sequence (5'-3') used in this study. * ^a | | |
|--|------------------------|--|
| eGFP | Forward _{Nat} | <u>ccccccat</u> atggtgagcaagggcgaggagc |
| | Reverse ₁ | ggtctggctc <u>gaggt</u> acagctcgtccatgcc |
| *: the restriction sites for NdeI (forward) and XhoI (reverse) are underlined. | | |

Bacterial cells were cultured as previously described.⁵⁵ Briefly, a single colony of bacteria carrying the pET23a(+)-eGFP plasmid was inoculated in Luria Bertani (LB) broth in the presence of Ampicillin (50 μ g/ml) and incubated overnight at 37 °C until stationary phase was reached. The bacterial culture was then diluted to OD₆₀₀ = 0.1 (1x10⁷ CFU ml⁻¹) in LB media supplemented with the same antibiotics. Then, each substrate was incubated with 5 ml of bacterial suspension and kept in 12-well culture plates. Finally, isopropyl-1-thio-D-galactopyranoside (IPTG) was added to the bacterial culture at a final concentration of 1 mM, following a 24-hours incubation at 25 C on a platform shaker. After 24 hours the samples were removed from the bacteria growing medium, washed 3 times with mQ-H₂O and covered with a drop of water. Fluorescence

1
2
3 1 images for the evaluation of the bacteria adhesion grade on the different substrates were acquired using an
4
5 2 inverted fluorescence microscope (Nikon Eclipse Ti), by exciting with a 470 nm light source (Lumencor
6
7 3 Spectra X) and using a standard FITC filters set. The average number of bacteria adhered on each substrate
8
9 4 type was quantified using Imagej software. Mean values were averaged over n = 10 fields of view for each
10
11 5 sample type, and over n = 3 statistically independent samples. For evaluating the bactericidal activity,
12
13 6 bacterial cells were cultured as described above. However, no IPTG was added into the bacterial solution.
14
15 7 The optical density of these solutions was measured at 600nm using a UV-Vis Spectrometer. Control
16
17 8 measurements on bacteria grown in the medium where no sample is present were carried out at the same
18
19 9 time.
20
21
22
23
24

25 11 **3. Results and Discussion**

27 12 **3.1. Fabrication of micro-patterned silk substrates**

29 13 We fabricate different micro- and nano-patterned silk fibroin substrates by employing a soft-lithography
30
31 14 approach.⁵¹ The procedure, sketched in **Figure 1**, starts with the extraction of the silk fibroin protein from
32
33 15 the *Bombyx mori* degummed silk fibers through dissolution in LiBr solution and subsequent dialysis against
34
35 16 ultrapure water. The silk fibroin solution is then drop casted on top of micro- and nano-patterned PDMS
36
37 17 molds. Once solidified, the fibroin films are subjected to water vapor annealing. This process increases the
38
39 18 crystallinity by promoting the formation of β -sheet dominated silk II structure, which is water insoluble.⁵⁴
40
41 19 Four types of surface morphology are obtained by replicating different PDMS molds: flat, nano stripes, small
42
43 20 μ wells and big μ wells. To obtain the PDMS mold for nano-striped silk, we replicated the grooved
44
45 21 polycarbonate layer of a CD-ROM, while for fabricating the micro-domes mold (negative morphology for
46
47 22 μ wells) we employed the nature-inspired templating process known as breath figure formation.⁵⁶ Therefore,
48
49 23 not only the preparation of silk substrates but the whole patterning process is achieved by affordable and
50
51 24 simple techniques based on self-assembly. For the flat controls, a flat PDMS layer is used. Silk fibroin solution
52
53 25 is initially processed into ~ 20 cm² films (Figure 1 top inset), which are then cut in 1.8 cm diameter disks for
54
55 26 performing the experiments (Figure 1 bottom inset). The thickness of the micro and nanopatterned silk films
56
57
58
59
60

1
2
3
4
5
6
7
8
9
10
11
12
13
14
15
16
17
18
19
20
21
22
23
24
25
26
27
28
29
30
31
32
33
34
35
36
37
38
39
40
41
42
43
44
45
46
47
48
49
50
51
52
53
54
55
56
57
58
59
60

1 is about 100 μm . Such a thickness is significantly higher than the height of the nano and micro features
2 present on the patterned silk surfaces. This fact suggests that the mechanical properties of the patterned
3 substrates are comparable to those reported in the literature for flat films obtained with the same fabrication
4 process.⁵⁴ Moreover, the micro and nanopatterned coatings do not negatively affect the silk mechanical
5 properties, since all reported patterned substrates can be easily bent at curvature angles $\gg 90^\circ$, even when
6 they are in the dry form and the wet coatings can be successfully wrapped on different curved objects (Figure
7 S1).

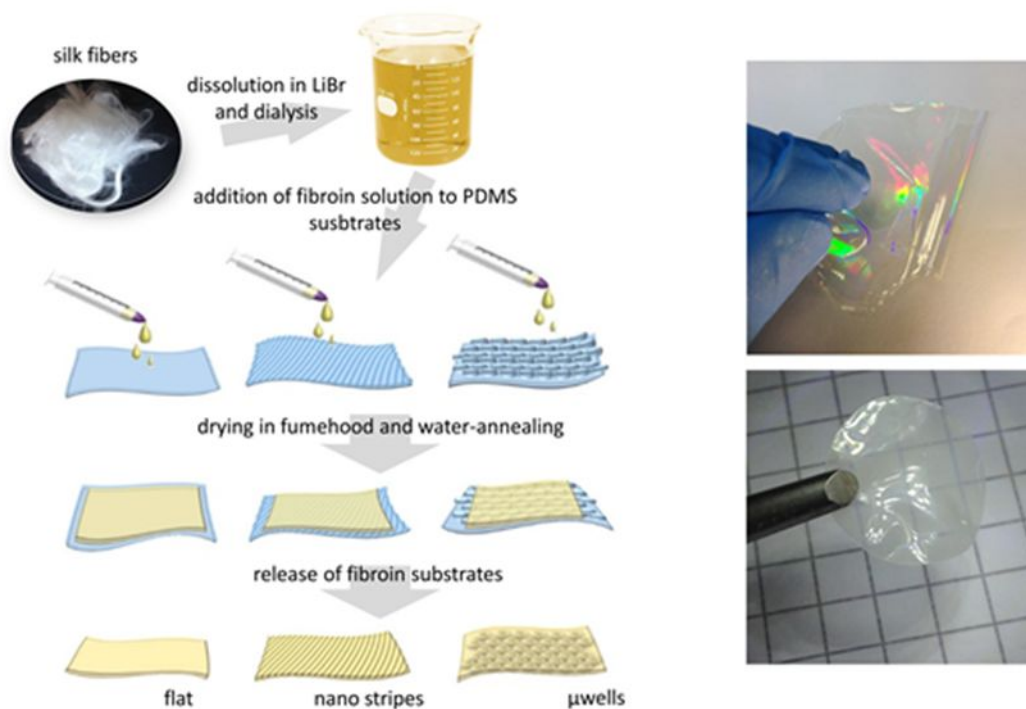


Figure 1. Silk substrates fabrication. A soft lithography and self-assembly approach allows for fast, scalable and highly repeatable fabrication of patterned silk substrates, with different design. In this case, nano stripes and micro wells with different diameters have been realized. In the inset: representative photographs of a patterned silk film before cutting (top) and a 1.8 cm diameter disk used for the assays (bottom).

Figure 2 shows the surface topography of the planar, unpatterned silk substrates (**Figure 2a**) and of micro/nano-structured samples with three different geometries (**Figure 2b-2d**), as obtained by acquiring SEM micrographs in top-view configuration. By employing different PDMS molds, three topographies are

1
2
3 1 obtained: (1) a nano stripes-patterned silk fibroin surface, composed by grooves of ~ 800 nm width and
4
5 2 spacing of the same dimension (nano stripes, **Figure 2b**); (2) silk fibroin micro wells of different diameters,
6
7 3 ranging from 3.5 to 5 μm ($\mu\text{wells 1}$, **Figure 2c**); (3) silk fibroin micro wells with a shape similar to $\mu\text{wells 1}$, but
8
9 4 lower diameter, in the range 1-2 μm ($\mu\text{wells 2}$, **Figure 2d**). The choice of these patterning geometries was
10
11 5 inspired by antifouling approaches adopted by nature systems,⁴⁷ as well as by existing literature reports
12
13 6 about biomimetic antifouling devices.^{39,42} In particular, nano stripes and $\mu\text{wells 2}$ follow the solution adopted,
14
15 7 for instance, in the shark skin, in which grooves width lower than bacterial dimension leads to inhibition of
16
17 8 biofilm formation. $\mu\text{wells 1}$ geometry instead was optimized in order to induce the formation of air pockets
18
19 9 within the microstructures, which was previously reported to substantially inhibit bacterial adhesion⁵⁷ and
20
21 10 recalls solutions adopted, for instance, in lotus leaf.⁴⁷ Silk substrates morphology is also characterized by AFM
22
23 11 (**Figure 2e-2h**). The surface roughness of the flat silk control substrates (**Figure 2e**) is in line with the existing
24
25 12 literature (root mean square roughness (RMS) value \pm standard error of the mean (s.e.m.), 0.86 ± 0.03 nm).⁵⁸
26
27 13 The average height of the micro-structured features amounts at 0.124 ± 0.005 μm , 1.06 ± 0.03 μm and
28
29 14 0.122 ± 0.007 μm (mean \pm s.e.m.) for the nano stripes, $\mu\text{wells 1}$ and $\mu\text{wells 2}$ cases respectively (**Figures 2f-**
30
31 15 **2h**).
32
33
34
35
36
37
38
39
40
41
42
43
44
45
46
47
48
49
50
51
52
53
54
55
56
57
58
59
60

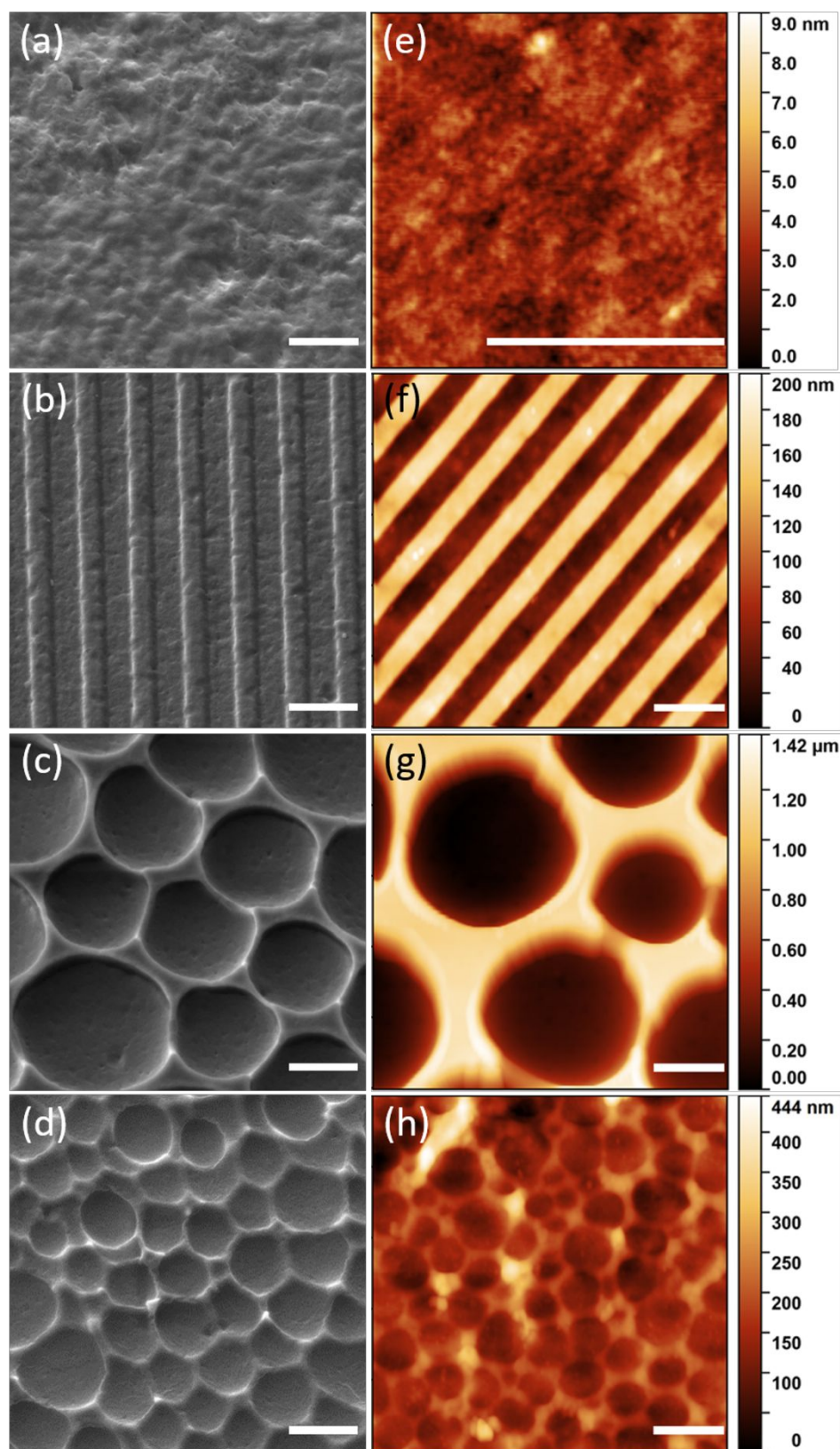


Figure 2. Topography of flat and micro/nano-patterned silk substrates. (a)-(d): SEM top-view images of silk flat (a), nano stripes (b), μ wells 1 (c) and μ wells 2 (d). Scale bars, 2 μ m. (e)-(h): AFM topography images of silk flat (e), nano stripes (f), μ wells 1 (g) and μ wells 2 (h) samples. Scale bars, 2 μ m.

3.2. HEK-293 cells cultures on micro/nano-patterned silk substrates

Once extracted from *Bombyx mori* silk following an established purification route,⁵⁹ silk fibroin shows optimal biocompatibility, as documented in several *in-vivo* and *in-vitro* studies.^{60–62} However, much less is known about the cytocompatibility of patterned silk fibroin substrates. Thus, by culturing HEK-293 cell models on top of the different micro- and nano- patterned silk fibroin-based substrates, we directly investigate whether structured surface topographies sizably affect the viability of living cells. Cell proliferation is monitored by performing the MTT assay (**Figure 3**). The method is based on the use of the water-soluble tetrazolium salt (MTT), which is metabolized/reduced by living cells into a water-insoluble formazan product. As the optical absorption of formazan, which has a characteristic purple color, is proportional to the number of living cells, it can be directly related to the cell viability and capability to proliferate. Formazan absorption in the MTT-treated cell cultures on the different morphologies is evaluated after 1, 3 and 4 days *in vitro* (DIV), showing no statistically significant differences between micro/nano-patterned and planar silk topographies cases (**Figure 3**). This clearly indicates that the micro and nanostructures do not substantially affect the viability and the proliferation of HEK-293 cells, despite the fact that cells may be subjected to a higher surface pressure due to the reduced contact area. Instead, conditions favorable to cell proliferation are established, as also reported by recent literature and attributed to the higher surface energy and subsequent superhydrophilicity typical of the silk substrate.⁴⁹ In our case, there are no significant differences between flat and patterned silk substrates, but this observation may critically depend on the considered cell model, and it should not be considered of general validity. Interestingly, an enhancement in the proliferation of cells that were seeded on nanopatterned silk was recently observed in the case of human adipose mesenchymal stem cells, which usually feature exquisite sensitivity to the underlying substrate topography.⁶³

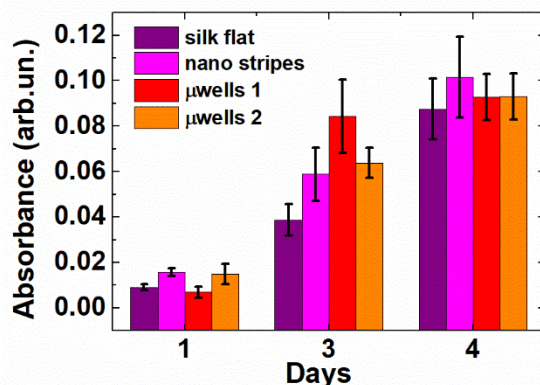


Figure 3. HEK-293 cells viability. MTT viability assay on HEK293 cells plated on top of the different silk substrates. Data are reported as mean \pm s.e.m. A one-way ANOVA followed by post-hoc Dunnett's correction analysis reveals that none of the patterned silk substrates present any statistically significant difference in comparison to the planar silk samples.

3.3. Evaluation of *Escherichia coli* adhesion on pristine and structured silk substrates

The antifouling capability of the different micro/nano-patterned silk samples is evaluated by employing the *E. coli* bacterial model, genetically modified to express green fluorescent protein (GFP), which is used as a visual marker. The substrates are incubated with the GFP-expressing *E. coli* for 24h, washed with ultrapure water for removing all unattached bacteria and covered with an ultrapure water drop. The number of adherent bacteria is then quantified by acquiring GFP fluorescence emission (**Figure 4a-4d**) using a fluorescence microscope. Measurements were acquired after 24 hours, when biofilm formation is known to be irreversible and fully completed.⁶⁴ All the silk samples display a lower number of adhered bacteria in comparison to the flat silk control. Importantly, the micro- and nano-patterned silk samples present a significant reduction in the number of *E. coli* attached to their surfaces in comparison with the flat silk morphology, amounting at 49 % ($p < 0.05$), 66 % ($p < 0.001$) and 64 % ($p < 0.01$) for the nano stripes, μ wells 1 and μ wells 2 cases respectively (**Figure 4e**). For completeness we verified by AFM that the patterning structures are preserved after exposure to the media employed for preparing the cell and bacterial cultures (Figure S2).

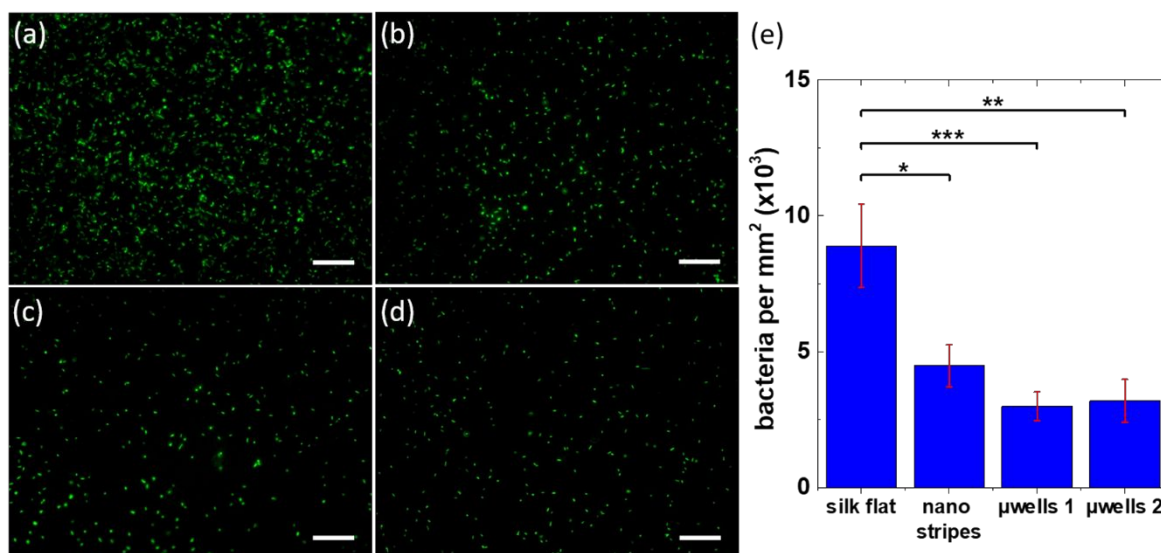


Figure 4. Evaluation of bacterial adhesion on patterned silk. Fluorescent microscopy images of GFP expressing bacteria cultured on flat (a), nano-striped (b), μ wells 1-patterned (c), μ wells 2-patterned (d) silk substrates, after 24h. Scale bars, 50 μ m. (e) Quantitative analysis of bacteria observed in a-d. * $p < 0.05$, ** $p < 0.01$, *** $p < 0.001$.

This result can be attributed to a topography-driven antifouling mechanism. In previous reports, two main effects were found to have a central role in the inhibition of bacterial adhesion: (1) a steric effect due to the presence of a regular micro-patterned morphology characterized by a features size lower than bacterial dimension,^{39,40,65} and (2) the hydrophobic effect induced by micro-structured surfaces.^{39,41,57,66} In both cases the driving force of the antifouling process relies on the reduction of the surface area to which the organisms can adhere. The reduced bacterial adhesion achieved with silk nano stripes and μ wells 2 can be explained by considering the former mechanism, since the *E. coli* average length ($\sim 2 \mu\text{m}$) and diameter ($\sim 1 \mu\text{m}$)^{67,68} are higher than the width of the nano stripes silk grooves ($\sim 800 \text{ nm}$), as well as the μ wells 2 mean diameter (between 1 and 2 μm). On the contrary, this argumentation is not valid for explaining the bacterial adhesion reduction induced by μ wells 1, because the diameter of the wells that compose this architecture (in the range between 3.5 and 5 μm) is about twice as large as the *E. coli* average dimension. In order to clarify the origin of the antifouling effect observed, experiments for the evaluation of the hydrophobicity of the samples are carried out by measuring the static contact angle of the considered surfaces (**Figure 5** and **Figure S3**).

1
2
3
4
5
6
7
8
9
10
11
12
13
14
15
16
17
18
19
20
21
22
23
24
25
26
27
28
29
30
31
32
33
34
35
36
37
38
39
40
41
42
43
44
45
46
47
48
49
50
51
52
53
54
55
56
57
58
59
60

Generally, the limit between hydrophilicity and hydrophobicity is placed at a contact angle value of 90° .⁶⁹ Planar silk is hydrophilic, presenting a water contact angle value of $69^\circ \pm 1^\circ$. Silk nano stripes and μ wells 2 samples show increased water contact angle values ($73^\circ \pm 0.5^\circ$ and $82^\circ \pm 2^\circ$ respectively), but they still fall in the hydrophilic regime, confirming that the observed decrease of *E. coli* adhesion is due to a steric effect exerted by the surface topography and it is not strictly related to the surface wettability. μ wells 1 substrates display instead a hydrophobic behavior, with a water contact angle of $100^\circ \pm 1^\circ$. This result is in line with the existing literature, where similar honeycomb surface topographies have been shown to influence the wettability of polymer films.^{57,70,71} In particular, this behavior has been explained by the formation of air pockets between the surface of the substrate and the water droplets, when the latter are much larger than the dimension of the structures present on the surface of the substrate.⁷⁰ This phenomenon could explain the μ wells 1 antifouling properties, since it directly determines the amount of surface that is available for bacterial attachment. Our interpretation of the results for μ wells 1 is also in line with the work by Manabe *et al.*, showing that when the size of the pores lies between 3.5 and 11 μm and the contact angle of the culture medium is high, bacteria experience a limited contact with the surface.⁵⁷

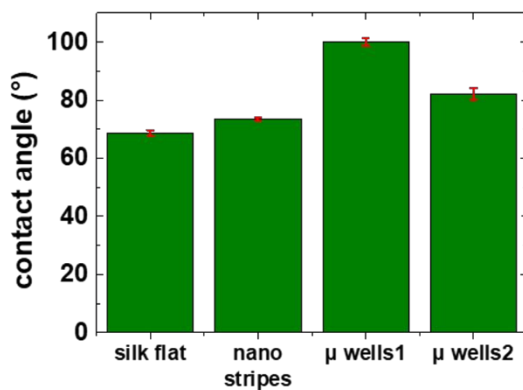
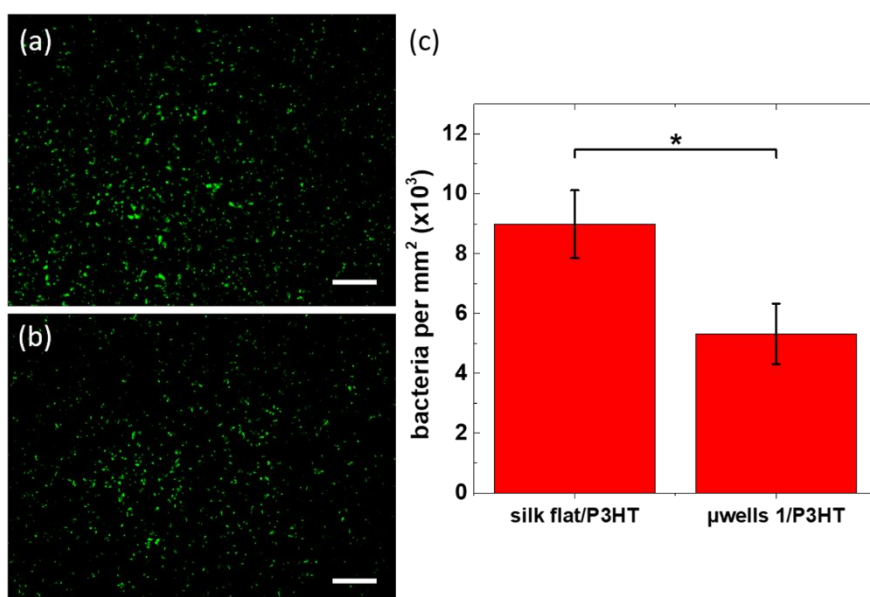


Figure 5. Water contact angle measurement. Static contact angles established by water drops over planar and micro/nano-patterned silk morphologies.

3.4. Evaluation of *E. Coli* adhesion on rr-P3HT-covered silk substrates

Among the numerous biotechnology applications of silk-based biomaterials, optics and biophotonics are emerging as some of the most attractive ones. Various types of implantable optical devices, including optical waveguides,^{14,72,73} optical fibers⁷⁴ and microprism arrays,^{75,76} based on biocompatible silk have been described in the literature.^{13,77} This is due to the silk's good optical transparency, which ensures a high refractive index and low optical losses, even when used within *in vivo* systems. Silk has also been recently used as a long-term biocompatible substrate in the fabrication of functionally autonomous photovoltaic visual prostheses.⁶² In this case, the excellent mechanical properties of silk were usefully coupled to the light responsivity and charge generation properties of a thiophene-based conjugated polymer, regio-regular poly(3-hexylthiophene-2,5-diyl) (rr-P3HT). It has been shown that a silk/polymer device is highly tolerated within the subretinal space of rats and partially recovers visual acuity in blind retinas.^{62,78,79} These seminal works demonstrated that silk-based biomaterials can be coupled to optically-active polymers, thus providing a vast array of opportunities for the development of light-based diagnostic and therapeutic tools. In view of its huge *in vivo* application potential, we set out to investigate whether the excellent antifouling efficacy shown by micro-structured silk substrates is preserved even in the presence of a thin film of a semiconducting polymer deposited on top of the surface. We focused our attention on the substrate that gave the best antifouling result, μ wells 1, and on the planar silk morphology as a control. The deposition of the layer of the semiconducting polymer is carried out by spin-coating, by selecting the proper rr-P3HT concentration and spin parameters that do not lead to a passivation of the micro-structured topography. Polymer thin film thickness is in the order of 30 nm, showing an optical absorption of ~ 0.3 , which ensures good charge generation efficiency and photovoltaic properties also when exposed to aqueous saline solutions and cell growth media.⁸⁰ SEM images of the rr-P3HT-covered/uncovered samples confirm that the honeycomb microstructure is not altered upon polymer deposition (**Figure S4**). Moreover, photographs and fluorescence images corroborate this picture and highlight the uniformity of the P3HT coverage (Figure S5). *E. coli* adhesion is evaluated in rr-P3HT-covered silk samples (**Figure 6**), after having verified their stability in the culture media (Figure S6). We notice that the average density of bacteria adherent to polymer-coated silk flat samples is

1
2
3 1 similar to the one recorded in uncoated samples (**Figure 4**), thus allowing us to exclude a concomitant
4
5 2 antifouling action due to the polymer thin film alone. We also notice that the hydrophobicity value typical of
6
7 3 rr-P3HT polymer thin films in dry conditions (about 100°) is substantially decreased when the polymer is
8
9 4 directly exposed to an aqueous environment, due to water permeation and ion doping, dropping up to 60°-
10
11 5 70°. ⁸¹ Thus, the polymer itself is not expected to sustain or to boost an antifouling effect. Importantly,
12
13 6 however, the μ wells 1/P3HT sample displays a reduction of 41 % ($p < 0.05$) in the adhesion of bacteria relative
14
15 7 to the flat control, thus demonstrating that the topography-driven antifouling effect of structured silk is
16
17 8 substantially preserved also in the presence of a thin film of a conjugated polymer deposited on top of its
18
19 9 upper, bacteria-exposed surface.



44
45 12 **Figure 6. Evaluation of bacteria adhesion.** Fluorescent microscopy images of GFP expressing bacteria
46
47 13 cultured on silk flat/P3HT (a) and μ wells 1/P3HT (b), after 24h. Scale bar 50 μ m. (c) Quantitative analysis of
48
49 14 bacteria observed in a,b. * $p < 0.05$.

50
51 15
52
53 16 In order to corroborate our findings, we carried out experiments aimed at the quantification of the
54
55 17 bacterial growth inside the culture medium in the presence of all the tested substrates, thus providing an
56
57 18 insight into the existence of possible sample-induced bactericidal effects. *E. coli* cultures are prepared in the
58
59 19 same way as in the antifouling experiments case, and the bacterial growth is evaluated by measuring the

1 culture medium optical absorption at 600 nm after 24h (**Figure 7**). The results show that there are no
2 significant differences between the case where no substrate is present and the one where bacteria are
3 incubated with both P3HT-uncovered (**Figure 7a**) and P3HT-covered (**Figure 7b**) silk samples. On the basis of
4 these findings we can conclude that the reduction of the surface-attached bacteria is only due to an
5 unfavorable bacterial adhesion induced by the micro/nano-patterned topographies and we can exclude a
6 bactericidal effect exerted by the micro/nano-patterned silk-based morphologies.

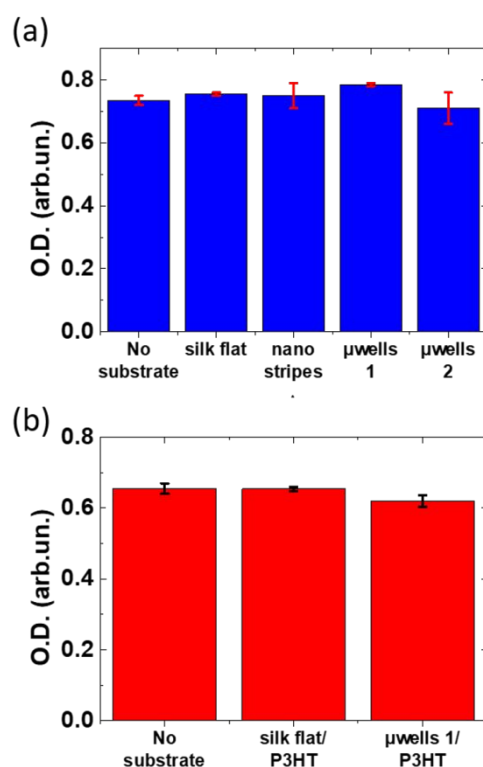


Figure 7. Evaluation of the antibacterial activity of the micro/nano-patterned silk-based substrates.

Bacterial growth in solution after 24h incubation with P3HT-uncovered (a) and P3HT-covered (b) silk substrates in comparison to the case where no substrate is present inside the growth medium. Bacterial growth is evaluated as the optical density (O.D.) at 600 nm.

Conclusions

A fast, facile and easily scalable processing method based on soft lithography is applied to realize nano- and micro-structured silk samples, with different geometries. We show that patterned silk substrates display excellent antifouling properties, leading in all cases to a substantial reduction of bacterial adhesion. At the

1
2
3 1 same time, we show that the well-known cytocompatibility properties, which have been widely assessed in
4
5 2 multiple studies for silk flat substrates, are fully preserved also in the case of silk microstructures. The
6
7 3 antifouling effect is explained on the basis of a complex interplay between geometrical constraints, as the
8
9 4 bacteria membrane has a lower surface area available for adhesion, and the enhancement of hydrophobicity
10
11 5 induced by microstructuring. In particular, we identify an optimal combination of the above mentioned
12
13 6 effects and we demonstrate that suitable silk patterning leads to a more than 65% decrease in bacteria
14
15 7 adhesion, as compared to flat silk substrates. As an important step towards the realization of fully-
16
17 8 biocompatible and functional devices for photo-medicine, we demonstrate that the antifouling properties of
18
19 9 patterned silk microstructures are fully preserved also in combination with a light-active conjugated polymer.
20
21 10 This paves the way towards the realization of a novel generation of bio-polymer implantable devices,
22
23 11 endowed with mechanical properties similar to those of biological tissues, and able to both optically
24
25 12 modulate/optically sense the activity of cells and to substantially inhibit biofilm formation.
26
27
28
29
30
31
32
33
34
35
36
37
38
39
40
41
42
43
44
45
46
47
48
49
50
51
52
53
54
55
56
57
58
59
60

1 **ASSOCIATED CONTENT**

2 **Supporting Information**

3 The following file is available free of charge. Representative photographs showing the micro/nano
4 patterned silk substrates in different configurations. AFM images showing the patterned silk topographies
5 after incubation in culture media. Representative photographs of water droplets in contact with the silk-
6 based substrates. SEM top-view images of the bare and P3HT-covered silk substrates. Representative
7 photographs and fluorescence images of the P3HT layer deposited on patterned silk. Representative
8 photographs and photoluminescence spectra of the P3HT-covered substrates after incubation in culture
9 media.

10 **AUTHOR INFORMATION**

11 Corresponding Author

12 *(MRA) E-mail: mariarosa.antognazza@iit.it

13 **AUTHORS CONTRIBUTION**

14 G.T., M.P., E.P., F.G. and M.R.A. planned the research. F.G. prepared the silk substrates. G.T. carried out SEM,
15 AFM with help from F.G., fluorescence microscopy, cells viability assay with help from F.L., and contact angle
16 measurements. S.D. prepared and characterized bacteria cultures. C.B. and F.L. helped with cell cultures
17 preparation. G.T. carried out data analysis. G.T. and M.R.A. interpreted the data and wrote the main
18 manuscript, with contribution from all authors. M.R.A. supervised the work. All authors approved the final
19 manuscript.

20 **FUNDING SOURCES**

21 MRA acknowledges support by the European Research Council (ERC) under the European Union's Horizon
22 2020 research and innovation program 'LINCE', grant agreement n. 803621. FL and MRA acknowledge
23 support by EU Horizon 2020 FETOPEN-2018-2020 Programme 'LION-HEARTED', grant agreement n. 828984.

24 **Competing interests:** The authors declare that they have no competing interests.

References

- 1
2
3 1
4 2
5 3 (1) Lawrence, B. D.; Marchant, J. K.; Pindrus, M. A.; Omenetto, F. G.; Kaplan, D. L. Silk Film Biomaterials
6 4 for Cornea Tissue Engineering. *Biomaterials* **2009**, *30* (7), 1299–1308.
7 5 <https://doi.org/10.1016/j.biomaterials.2008.11.018>.
- 8 6 (2) Kim, H. J.; Kim, U.-J.; Kim, H. S.; Li, C.; Wada, M.; Leisk, G. G.; Kaplan, D. L. Bone Tissue Engineering
9 7 with Premineralized Silk Scaffolds. *Bone* **2008**, *42* (6), 1226–1234.
10 8 <https://doi.org/10.1016/j.bone.2008.02.007>.
- 11 9 (3) Fuchs, S.; Jiang, X.; Schmidt, H.; Dohle, E.; Ghanaati, S.; Orth, C.; Hofmann, A.; Motta, A.; Migliaresi,
12 10 C.; Kirkpatrick, C. J. Dynamic Processes Involved in the Pre-Vascularization of Silk Fibroin Constructs
13 11 for Bone Regeneration Using Outgrowth Endothelial Cells. *Biomaterials* **2009**, *30* (7), 1329–1338.
14 12 <https://doi.org/10.1016/j.biomaterials.2008.11.028>.
- 15 13 (4) Unger, R. Growth of Human Cells on a Non-Woven Silk Fibroin Net: A Potential for Use in Tissue
16 14 Engineering. *Biomaterials* **2004**, *25* (6), 1069–1075. [https://doi.org/10.1016/S0142-9612\(03\)00619-7](https://doi.org/10.1016/S0142-9612(03)00619-7).
- 17 15 (5) Wang, Y.; Bella, E.; Lee, C. S. D.; Migliaresi, C.; Pelcastre, L.; Schwartz, Z.; Boyan, B. D.; Motta, A. The
18 16 Synergistic Effects of 3-D Porous Silk Fibroin Matrix Scaffold Properties and Hydrodynamic
19 17 Environment in Cartilage Tissue Regeneration. *Biomaterials* **2010**, *31* (17), 4672–4681.
20 18 <https://doi.org/10.1016/j.biomaterials.2010.02.006>.
- 21 19 (6) Guarino, V.; Benfenati, V.; Cruz-Maya, I.; Saracino, E.; Zamboni, R.; Ambrosio, L. Instructive Proteins
22 20 for Tissue Regeneration. In *Functional 3D Tissue Engineering Scaffolds*; Elsevier, 2018; pp 23–49.
23 21 <https://doi.org/10.1016/B978-0-08-100979-6.00002-1>.
- 24 22 (7) Pistone, A.; Sagnella, A.; Chieco, C.; Bertazza, G.; Varchi, G.; Formaggio, F.; Posati, T.; Saracino, E.;
25 23 Caprini, M.; Bonetti, S.; Toffanin, S.; Di Virgilio, N.; Muccini, M.; Rossi, F.; Ruani, G.; Zamboni, R.;
26 24 Benfenati, V. Silk Fibroin Film from Golden-Yellow *Bombyx Mori* Is a Biocomposite That Contains
27 25 Lutein and Promotes Axonal Growth of Primary Neurons: Yellow SF in the Field of
28 26 Neuroregenerative Medicine. *Biopolymers* **2016**, *105* (5), 287–299.
29 27 <https://doi.org/10.1002/bip.22806>.
- 30 28 (8) Koh, L.-D.; Yeo, J.; Lee, Y. Y.; Ong, Q.; Han, M.; Tee, B. C.-K. Advancing the Frontiers of Silk Fibroin
31 29 Protein-Based Materials for Futuristic Electronics and Clinical Wound-Healing (Invited Review).
32 30 *Mater. Sci. Eng. C* **2018**, *86*, 151–172. <https://doi.org/10.1016/j.msec.2018.01.007>.
- 33 31 (9) Suzuki, S.; Shadforth, A. M. A.; McLenachan, S.; Zhang, D.; Chen, S.-C.; Walshe, J.; Lidgerwood, G. E.;
34 32 Pébay, A.; Chirila, T. V.; Chen, F. K.; Harkin, D. G. Optimization of Silk Fibroin Membranes for Retinal
35 33 Implantation. *Mater. Sci. Eng. C* **2019**, *105*, 110131. <https://doi.org/10.1016/j.msec.2019.110131>.
- 36 34 (10) Germershaus, O.; Werner, V.; Kutscher, M.; Meinel, L. Deciphering the Mechanism of Protein
37 35 Interaction with Silk Fibroin for Drug Delivery Systems. *Biomaterials* **2014**, *35* (10), 3427–3434.
38 36 <https://doi.org/10.1016/j.biomaterials.2013.12.083>.
- 39 37 (11) Meinel, L.; Kaplan, D. L. Silk Constructs for Delivery of Musculoskeletal Therapeutics. *Adv. Drug Deliv.*
40 38 *Rev.* **2012**, *64* (12), 1111–1122. <https://doi.org/10.1016/j.addr.2012.03.016>.
- 41 39 (12) Li, A. B.; Kluge, J. A.; Guziewicz, N. A.; Omenetto, F. G.; Kaplan, D. L. Silk-Based Stabilization of
42 40 Biomacromolecules. *J. Controlled Release* **2015**, *219*, 416–430.
43 41 <https://doi.org/10.1016/j.jconrel.2015.09.037>.
- 44 42 (13) Humar, M.; Kwok, S. J. J.; Choi, M.; Yetisen, A. K.; Cho, S.; Yun, S.-H. Toward Biomaterial-Based
45 43 Implantable Photonic Devices. *Nanophotonics* **2017**, *6* (2). <https://doi.org/10.1515/nanoph-2016-0003>.
46 44
47 45
48
49
50
51
52
53
54
55
56
57
58
59
60

- 1
2
3 1 (14) Parker, S. T.; Domachuk, P.; Amsden, J.; Bressner, J.; Lewis, J. A.; Kaplan, D. L.; Omenetto, F. G.
4 2 Biocompatible Silk Printed Optical Waveguides. *Adv. Mater.* **2009**, *21* (23), 2411–2415.
5 3 <https://doi.org/10.1002/adma.200801580>.
6 4 (15) Tsiaris, K.; Tilburey, G. E.; Murphy, A. R.; Domachuk, P.; Kaplan, D. L.; Omenetto, F. G.
7 5 Functionalized-Silk-Based Active Optofluidic Devices. *Adv. Funct. Mater.* **2010**, *20* (7), 1083–1089.
8 6 <https://doi.org/10.1002/adfm.200902050>.
9 7 (16) Benfenati, V.; Zamboni, R. Silk Biomaterials Enable Living Technologies Targeting Brain Cells.
10 8 *Nonlinear Opt. Quantum Opt. Concepts Mod. Opt.* **2019**, *50*, 183–201.
11 9 (17) Sagnella, A.; Zambianchi, M.; Durso, M.; Posati, T.; Del Rio, A.; Donnadio, A.; Mazzanti, A.; Pistone,
12 10 A.; Ruani, G.; Zamboni, R.; Benfenati, V.; Melucci, M. APTES Mediated Modular Modification of
13 11 Regenerated Silk Fibroin in a Water Solution. *RSC Adv.* **2015**, *5* (78), 63401–63406.
14 12 <https://doi.org/10.1039/C5RA10016J>.
15 13 (18) Tao, H.; Kainerstorfer, J. M.; Siebert, S. M.; Pritchard, E. M.; Sassaroli, A.; Panilaitis, B. J. B.; Brenckle,
16 14 M. A.; Amsden, J. J.; Levitt, J.; Fantini, S.; Kaplan, D. L.; Omenetto, F. G. Implantable, Multifunctional,
17 15 Bioresorbable Optics. *Proc. Natl. Acad. Sci.* **2012**, *109* (48), 19584–19589.
18 16 <https://doi.org/10.1073/pnas.1209056109>.
19 17 (19) Shimanovich, U.; Pinotsi, D.; Shimanovich, K.; Yu, N.; Bolisetty, S.; Adamcik, J.; Mezzenga, R.;
20 18 Charmet, J.; Vollrath, F.; Gazit, E.; Dobson, C. M.; Kaminski Schierle, G.; Holland, C.; Kaminski, C. F.;
21 19 Knowles, T. P. J. Biophotonics of Native Silk Fibrils. *Macromol. Biosci.* **2018**, *18* (4), 1700295.
22 20 <https://doi.org/10.1002/mabi.201700295>.
23 21 (20) Shan, D.; Gerhard, E.; Zhang, C.; Tierney, J. W.; Xie, D.; Liu, Z.; Yang, J. Polymeric Biomaterials for
24 22 Biophotonic Applications. *Bioact. Mater.* **2018**, *3* (4), 434–445.
25 23 <https://doi.org/10.1016/j.bioactmat.2018.07.001>.
26 24 (21) Zhang, Y.; Zhou, Z.; Fan, Z.; Zhang, S.; Zheng, F.; Liu, K.; Zhang, Y.; Shi, Z.; Chen, L.; Li, X.; Mao, Y.;
27 25 Wang, F.; Sun, Y.-L.; Tao, T. H. Self-Powered Multifunctional Transient Bioelectronics. *Small* **2018**, *14*
28 26 (35), 1802050. <https://doi.org/10.1002/sml.201802050>.
29 27 (22) Chatterjee, S.; Saxena, M.; Padmanabhan, D.; Jayachandra, M.; Pandya, H. J. Futuristic Medical
30 28 Implants Using Bioresorbable Materials and Devices. *Biosens. Bioelectron.* **2019**, *142*, 111489.
31 29 <https://doi.org/10.1016/j.bios.2019.111489>.
32 30 (23) Hou, C.; Xu, Z.; Qiu, W.; Wu, R.; Wang, Y.; Xu, Q.; Liu, X. Y.; Guo, W. A Biodegradable and Stretchable
33 31 Protein-Based Sensor as Artificial Electronic Skin for Human Motion Detection. *Small* **2019**, *15* (11),
34 32 1805084. <https://doi.org/10.1002/sml.201805084>.
35 33 (24) Tao, H.; Hwang, S.-W.; Marelli, B.; An, B.; Moreau, J. E.; Yang, M.; Brenckle, M. A.; Kim, S.; Kaplan, D.
36 34 L.; Rogers, J. A.; Omenetto, F. G. Silk-Based Resorbable Electronic Devices for Remotely Controlled
37 35 Therapy and in Vivo Infection Abatement. *Proc. Natl. Acad. Sci.* **2014**, *111* (49), 17385–17389.
38 36 <https://doi.org/10.1073/pnas.1407743111>.
39 37 (25) Zhou, Z.; Shi, Z.; Cai, X.; Zhang, S.; Corder, S. G.; Li, X.; Zhang, Y.; Zhang, G.; Chen, L.; Liu, M.; Kaplan,
40 38 D. L.; Omenetto, F. G.; Mao, Y.; Tao, Z.; Tao, T. H. The Use of Functionalized Silk Fibroin Films as a
41 39 Platform for Optical Diffraction-Based Sensing Applications. *Adv. Mater.* **2017**, *29* (15), 1605471.
42 40 <https://doi.org/10.1002/adma.201605471>.
43 41 (26) Seo, J.-W.; Kim, H.; Kim, K.; Choi, S. Q.; Lee, H. J. Calcium-Modified Silk as a Biocompatible and Strong
44 42 Adhesive for Epidermal Electronics. *Adv. Funct. Mater.* **2018**, *28* (36), 1800802.
45 43 <https://doi.org/10.1002/adfm.201800802>.
46 44 (27) Huang, X. *Bioresorbable Materials and Their Application in Electronics*; Cambridge University Press,
47 45 2017.
48 46 (28) Kim, D.-H.; Viventi, J.; Amsden, J. J.; Xiao, J.; Vigeland, L.; Kim, Y.-S.; Blanco, J. A.; Panilaitis, B.;
49 47 Frechette, E. S.; Contreras, D.; Kaplan, D. L.; Omenetto, F. G.; Huang, Y.; Hwang, K.-C.; Zakin, M. R.;
50
51
52
53
54
55
56
57
58
59
60

1
2
3
4
5
6
7
8
9
10
11
12
13
14
15
16
17
18
19
20
21
22
23
24
25
26
27
28
29
30
31
32
33
34
35
36
37
38
39
40
41
42
43
44
45
46
47
48
49
50
51
52
53
54
55
56
57
58
59
60

- Litt, B.; Rogers, J. A. Dissolvable Films of Silk Fibroin for Ultrathin Conformal Bio-Integrated Electronics. *Nat. Mater.* **2010**, *9* (6), 511–517. <https://doi.org/10.1038/nmat2745>.
- (29) Tao, H.; Brenckle, M. A.; Yang, M.; Zhang, J.; Liu, M.; Siebert, S. M.; Averitt, R. D.; Mannoor, M. S.; McAlpine, M. C.; Rogers, J. A.; Kaplan, D. L.; Omenetto, F. G. Silk-Based Conformal, Adhesive, Edible Food Sensors. *Adv. Mater.* **2012**, *24* (8), 1067–1072. <https://doi.org/10.1002/adma.201103814>.
- (30) Cha, G. D.; Kang, D.; Lee, J.; Kim, D. Bioresorbable Electronic Implants: History, Materials, Fabrication, Devices, and Clinical Applications. *Adv. Healthc. Mater.* **2019**, *8* (11), 1801660. <https://doi.org/10.1002/adhm.201801660>.
- (31) Zhou, Z.; Zhang, S.; Cao, Y.; Marelli, B.; Xia, X.; Tao, T. H. Engineering the Future of Silk Materials through Advanced Manufacturing. *Adv. Mater.* **2018**, *30* (33), 1706983. <https://doi.org/10.1002/adma.201706983>.
- (32) Gomes, S. C.; Leonor, I. B.; Mano, J. F.; Reis, R. L.; Kaplan, D. L. Antimicrobial Functionalized Genetically Engineered Spider Silk. *Biomaterials* **2011**, *32* (18), 4255–4266. <https://doi.org/10.1016/j.biomaterials.2011.02.040>.
- (33) Nilebäck, L.; Hedin, J.; Widhe, M.; Floderus, L. S.; Krona, A.; Bysell, H.; Hedhammar, M. Self-Assembly of Recombinant Silk as a Strategy for Chemical-Free Formation of Bioactive Coatings: A Real-Time Study. *Biomacromolecules* **2017**, *18* (3), 846–854. <https://doi.org/10.1021/acs.biomac.6b01721>.
- (34) Lu, Z.; Xiao, J.; Wang, Y.; Meng, M. In Situ Synthesis of Silver Nanoparticles Uniformly Distributed on Polydopamine-Coated Silk Fibers for Antibacterial Application. *J. Colloid Interface Sci.* **2015**, *452*, 8–14. <https://doi.org/10.1016/j.jcis.2015.04.015>.
- (35) Zhou, W.; Jia, Z.; Xiong, P.; Yan, J.; Li, Y.; Li, M.; Cheng, Y.; Zheng, Y. Bioinspired and Biomimetic AgNPs/Gentamicin-Embedded Silk Fibroin Coatings for Robust Antibacterial and Osteogenic Applications. *ACS Appl. Mater. Interfaces* **2017**, *9* (31), 25830–25846. <https://doi.org/10.1021/acsami.7b06757>.
- (36) Grainger, D. W.; van der Mei, H. C.; Jutte, P. C.; van den Dungen, J. J. A. M.; Schultz, M. J.; van der Laan, B. F. A. M.; Zaat, S. A. J.; Busscher, H. J. Critical Factors in the Translation of Improved Antimicrobial Strategies for Medical Implants and Devices. *Biomaterials* **2013**, *34* (37), 9237–9243. <https://doi.org/10.1016/j.biomaterials.2013.08.043>.
- (37) Costerton, J. W. Bacterial Biofilms: A Common Cause of Persistent Infections. *Science* **1999**, *284* (5418), 1318–1322. <https://doi.org/10.1126/science.284.5418.1318>.
- (38) Jaggessar, A.; Shahali, H.; Mathew, A.; Yarlagadda, P. K. D. V. Bio-Mimicking Nano and Micro-Structured Surface Fabrication for Antibacterial Properties in Medical Implants. *J. Nanobiotechnology* **2017**, *15* (1). <https://doi.org/10.1186/s12951-017-0306-1>.
- (39) Katsikogianni, M. G.; Wood, D. J.; Missirlis, Y. F. Biomaterial Functionalized Surfaces for Reducing Bacterial Adhesion and Infection. In *Handbook of Bioceramics and Biocomposites*; Antoniac, I. V., Ed.; Springer International Publishing: Cham, 2015; pp 1–28. https://doi.org/10.1007/978-3-319-09230-0_32-1.
- (40) Nir, S.; Reches, M. Bio-Inspired Antifouling Approaches: The Quest towards Non-Toxic and Non-Biocidal Materials. *Curr. Opin. Biotechnol.* **2016**, *39*, 48–55. <https://doi.org/10.1016/j.copbio.2015.12.012>.
- (41) Bixler, G. D.; Theiss, A.; Bhushan, B.; Lee, S. C. Anti-Fouling Properties of Microstructured Surfaces Bio-Inspired by Rice Leaves and Butterfly Wings. *J. Colloid Interface Sci.* **2014**, *419*, 114–133. <https://doi.org/10.1016/j.jcis.2013.12.019>.
- (42) Magin, C. M.; Cooper, S. P.; Brennan, A. B. Non-Toxic Antifouling Strategies. *Mater. Today* **2010**, *13* (4), 36–44.

- 1
2
3 1 (43) Edwards, K. J.; Rutenberg, A. D. Microbial Response to Surface Microtopography: The Role of
4 2 Metabolism in Localized Mineral Dissolution. *Chem. Geol.* **2001**, *180* (1–4), 19–32.
5 3 [https://doi.org/10.1016/S0009-2541\(01\)00303-5](https://doi.org/10.1016/S0009-2541(01)00303-5).
6 4 (44) Anselme, K.; Davidson, P.; Popa, A. M.; Giazzon, M.; Liley, M.; Ploux, L. The Interaction of Cells and
7 5 Bacteria with Surfaces Structured at the Nanometre Scale. *Acta Biomater.* **2010**, *6* (10), 3824–3846.
8 6 <https://doi.org/10.1016/j.actbio.2010.04.001>.
9 7 (45) Zhao, N.; Wang, Z.; Cai, C.; Shen, H.; Liang, F.; Wang, D.; Wang, C.; Zhu, T.; Guo, J.; Wang, Y.; Liu, X.;
10 8 Duan, C.; Wang, H.; Mao, Y.; Jia, X.; Dong, H.; Zhang, X.; Xu, J. Bioinspired Materials: From Low to
11 9 High Dimensional Structure. *Adv. Mater.* **2014**, *26* (41), 6994–7017.
12 10 <https://doi.org/10.1002/adma.201401718>.
13 11 (46) Damodaran, V. B.; Murthy, N. S. Bio-Inspired Strategies for Designing Antifouling Biomaterials.
14 12 *Biomater. Res.* **2016**, *20* (1). <https://doi.org/10.1186/s40824-016-0064-4>.
15 13 (47) Bixler, G. D.; Bhushan, B. Rice and Butterfly Wing Effect Inspired Low Drag and Antifouling Surfaces:
16 14 A Review. *Crit. Rev. Solid State Mater. Sci.* **2015**, *40* (1), 1–37.
17 15 <https://doi.org/10.1080/10408436.2014.917368>.
18 16 (48) Wu, J.-G.; Chen, J.-H.; Liu, K.-T.; Luo, S.-C. Engineering Antifouling Conducting Polymers for Modern
19 17 Biomedical Applications. *ACS Appl. Mater. Interfaces* **2019**, *11* (24), 21294–21307.
20 18 <https://doi.org/10.1021/acsami.9b04924>.
21 19 (49) Mehrjou, B.; Mo, S.; Dehghan-Baniani, D.; Wang, G.; Qasim, A. M.; Chu, P. K. Antibacterial and
22 20 Cytocompatible Nanoengineered Silk-Based Materials for Orthopedic Implants and Tissue
23 21 Engineering. *ACS Appl. Mater. Interfaces* **2019**, *11* (35), 31605–31614.
24 22 <https://doi.org/10.1021/acsami.9b09066>.
25 23 (50) Lou, H.-Y.; Zhao, W.; Li, X.; Duan, L.; Powers, A.; Akamatsu, M.; Santoro, F.; McGuire, A. F.; Cui, Y.;
26 24 Drubin, D. G.; Cui, B. Membrane Curvature Underlies Actin Reorganization in Response to Nanoscale
27 25 Surface Topography. *Proc. Natl. Acad. Sci.* **2019**, *116* (46), 23143–23151.
28 26 <https://doi.org/10.1073/pnas.1910166116>.
29 27 (51) Galeotti, F.; Andicsova, A.; Yunus, S.; Botta, C. Precise Surface Patterning of Silk Fibroin Films by
30 28 Breath Figures. *Soft Matter* **2012**, *8* (17), 4815–4821. <https://doi.org/10.1039/C2SM25089F>.
31 29 (52) Galeotti, F.; Hartmann, L.; Botta, C. Robust Surface Patterning by Parylene-Reinforced Breath
32 30 Figures: An Enabling Tool for Liquid Crystal Microcell Arrays. *J. Colloid Interface Sci.* **2016**, *465*, 47–
33 31 53. <https://doi.org/10.1016/j.jcis.2015.11.053>.
34 32 (53) Galeotti, F.; Trespidi, F.; Timò, G.; Pasini, M. Broadband and Crack-Free Antireflection Coatings by
35 33 Self-Assembled Moth Eye Patterns. *ACS Appl. Mater. Interfaces* **2014**, *6* (8), 5827–5834.
36 34 <https://doi.org/10.1021/am500687f>.
37 35 (54) Hu, X.; Shmelev, K.; Sun, L.; Gil, E.-S.; Park, S.-H.; Cebe, P.; Kaplan, D. L. Regulation of Silk Material
38 36 Structure by Temperature-Controlled Water Vapor Annealing. *Biomacromolecules* **2011**, *12* (5),
39 37 1686–1696. <https://doi.org/10.1021/bm200062a>.
40 38 (55) Wang, L.-S.; Gupta, A.; Duncan, B.; Ramanathan, R.; Yazdani, M.; Rotello, V. M. Biocidal and
41 39 Antifouling Chlorinated Protein Films. *ACS Biomater. Sci. Eng.* **2016**, *2* (11), 1862–1866.
42 40 <https://doi.org/10.1021/acsbiomaterials.6b00464>.
43 41 (56) Zhang, A.; Bai, H.; Li, L. Breath Figure: A Nature-Inspired Preparation Method for Ordered Porous
44 42 Films. *Chem. Rev.* **2015**, *115* (18), 9801–9868. <https://doi.org/10.1021/acs.chemrev.5b00069>.
45 43 (57) Manabe, K.; Nishizawa, S.; Shiratori, S. Porous Surface Structure Fabricated by Breath Figures That
46 44 Suppresses *Pseudomonas Aeruginosa* Biofilm Formation. *ACS Appl. Mater. Interfaces* **2013**, *5* (22),
47 45 11900–11905. <https://doi.org/10.1021/am4035762>.
48
49
50
51
52
53
54
55
56
57
58
59
60

1

2

3

4

5

6

7

8

9

10

11

12

13

14

15

16

17

18

19

20

21

22

23

24

25

26

27

28

29

30

31

32

33

34

35

36

37

38

39

40

41

42

43

44

45

46

47

48

49

50

51

52

53

54

55

56

57

58

59

60

- (58) Lawrence, B. D.; Omenetto, F.; Chui, K.; Kaplan, D. L. Processing Methods to Control Silk Fibroin Film Biomaterial Features. *J. Mater. Sci.* **2008**, *43* (21), 6967–6985. <https://doi.org/10.1007/s10853-008-2961-y>.
- (59) Lawrence, B. D.; Pan, Z.; Weber, M. D.; Kaplan, D. L.; Rosenblatt, M. I. Silk Film Culture System for in Vitro Analysis and Biomaterial Design. *J. Vis. Exp.* 2012, No. 62, e3646. <https://doi.org/10.3791/3646>.
- (60) Meinel, L.; Hofmann, S.; Karageorgiou, V.; Kirker-Head, C.; McCool, J.; Gronowicz, G.; Zichner, L.; Langer, R.; Vunjak-Novakovic, G.; Kaplan, D. L. The Inflammatory Responses to Silk Films in Vitro and in Vivo. *Biomaterials* **2005**, *26* (2), 147–155. <https://doi.org/10.1016/j.biomaterials.2004.02.047>.
- (61) Yang, Y.; Chen, X.; Ding, F.; Zhang, P.; Liu, J.; Gu, X. Biocompatibility Evaluation of Silk Fibroin with Peripheral Nerve Tissues and Cells in Vitro. *Biomaterials* **2007**, *28* (9), 1643–1652. <https://doi.org/10.1016/j.biomaterials.2006.12.004>.
- (62) Antognazza, M. R.; Di Paolo, M.; Ghezzi, D.; Mete, M.; Di Marco, S.; Maya-Vetencourt, J. F.; Maccarone, R.; Desii, A.; Di Fonzo, F.; Bramini, M.; Russo, A.; Laudato, L.; Donelli, I.; Cilli, M.; Freddi, G.; Pertile, G.; Lanzani, G.; Bisti, S.; Benfenati, F. Characterization of a Polymer-Based, Fully Organic Prosthesis for Implantation into the Subretinal Space of the Rat. *Adv. Healthc. Mater.* **2016**, *5* (17), 2271–2282. <https://doi.org/10.1002/adhm.201600318>.
- (63) Ding, S.; Kingshott, P.; Thissen, H.; Pera, M.; Wang, P.-Y. Modulation of Human Mesenchymal and Pluripotent Stem Cell Behavior Using Biophysical and Biochemical Cues: A Review. *Biotechnol. Bioeng.* **2017**, *114* (2), 260–280. <https://doi.org/10.1002/bit.26075>.
- (64) Koseoglu, H.; Aslan, G.; Esen, N.; Sen, B. H.; Coban, H. Ultrastructural Stages of Biofilm Development of Escherichia Coli on Urethral Catheters and Effects of Antibiotics on Biofilm Formation. *Urology* **2006**, *68* (5), 942–946. <https://doi.org/10.1016/j.urology.2006.06.008>.
- (65) Bazaka, K.; Crawford, R. J.; Ivanova, E. P. Do Bacteria Differentiate between Degrees of Nanoscale Surface Roughness? *Biotechnol. J.* **2011**, *6* (9), 1103–1114. <https://doi.org/10.1002/biot.201100027>.
- (66) Watson, G. S.; Green, D. W.; Schwarzkopf, L.; Li, X.; Cribb, B. W.; Myhra, S.; Watson, J. A. A Gecko Skin Micro/Nano Structure – A Low Adhesion, Superhydrophobic, Anti-Wetting, Self-Cleaning, Biocompatible, Antibacterial Surface. *Acta Biomater.* **2015**, *21*, 109–122. <https://doi.org/10.1016/j.actbio.2015.03.007>.
- (67) Nelson, D. E.; Young, K. D. Penicillin Binding Protein 5 Affects Cell Diameter, Contour, and Morphology of Escherichia Coli. *J. Bacteriol.* **2000**, *182* (6), 1714–1721. <https://doi.org/10.1128/JB.182.6.1714-1721.2000>.
- (68) Grossman, N.; Ron, E. Z.; Woldringh, C. L. Changes in Cell Dimensions During Amino Acid Starvation of Escherichia Coli. *J BACTERIOL* **1982**, *152*, 7.
- (69) Förch, R.; Schönherr, H.; Schönherr, H.; Jenkins, A. T. A. *Surface Design: Applications in Bioscience and Nanotechnology*; John Wiley & Sons, 2009.
- (70) Wu, X.; Wang, S. Regulating MC3T3-E1 Cells on Deformable Poly(ϵ -Caprolactone) Honeycomb Films Prepared Using a Surfactant-Free Breath Figure Method in a Water-Miscible Solvent. *ACS Appl. Mater. Interfaces* **2012**, *4* (9), 4966–4975. <https://doi.org/10.1021/am301334s>.
- (71) Brown, P. S.; Talbot, E. L.; Wood, T. J.; Bain, C. D.; Badyal, J. P. S. Superhydrophobic Hierarchical Honeycomb Surfaces. *Langmuir* **2012**, *28* (38), 13712–13719. <https://doi.org/10.1021/la302719m>.
- (72) Sykes, E. A.; Albanese, A.; Chan, W. C. W. Implantable Waveguides. *Nat. Photonics* **2013**, *7* (12), 940–941. <https://doi.org/10.1038/nphoton.2013.308>.
- (73) Qiao, X.; Qian, Z.; Li, J.; Sun, H.; Han, Y.; Xia, X.; Zhou, J.; Wang, C.; Wang, Y.; Wang, C. Synthetic Engineering of Spider Silk Fiber as Implantable Optical Waveguides for Low-Loss Light Guiding. *ACS Appl. Mater. Interfaces* **2017**, *9* (17), 14665–14676. <https://doi.org/10.1021/acsami.7b01752>.

- 1
2
3 1 (74) Huby, N.; Vié, V.; Renault, A.; Beaufils, S.; Lefèvre, T.; Paquet-Mercier, F.; Pézolet, M.; Bêche, B.
4 2 Native Spider Silk as a Biological Optical Fiber. *Appl. Phys. Lett.* **2013**, *102* (12), 123702.
5 3 <https://doi.org/10.1063/1.4798552>.
6 4 (75) Lawrence, B. D.; Cronin-Golomb, M.; Georgakoudi, I.; Kaplan, D. L.; Omenetto, F. G. Bioactive Silk
7 5 Protein Biomaterial Systems for Optical Devices. *Biomacromolecules* **2008**, *9* (4), 1214–1220.
8 6 <https://doi.org/10.1021/bm701235f>.
9 7 (76) Tao, H.; Siebert, S. M.; Pritchard, E. M.; Sassaroli, A.; Panilaitis, B.; Brenckle, M. A.; Amsden, J. J.;
10 8 Levitt, J. M.; Fantini, S.; Kaplan, D. L.; Omenetto, F. G. Implantable Resorbable Micro-Prism Arrays for
11 9 Real-Time Drug Release Monitoring. In *Conference on Lasers and Electro-Optics 2012*; OSA: San Jose,
12 10 California, 2012; p CTh4L.8. https://doi.org/10.1364/CLEO_SI.2012.CTh4L.8.
13 11 (77) Omenetto, F. G.; Kaplan, D. L. A New Route for Silk. *Nat. Photonics* **2008**, *2* (11), 641–643.
14 12 <https://doi.org/10.1038/nphoton.2008.207>.
15 13 (78) Maya-Vetencourt, J. F.; Ghezzi, D.; Antognazza, M. R.; Colombo, E.; Mete, M.; Feyen, P.; Desii, A.;
16 14 Buschiazzo, A.; Di Paolo, M.; Di Marco, S.; Ticconi, F.; Emionite, L.; Shmal, D.; Marini, C.; Donelli, I.;
17 15 Freddi, G.; Maccarone, R.; Bisti, S.; Sambuceti, G.; Pertile, G.; Lanzani, G.; Benfenati, F. A Fully
18 16 Organic Retinal Prosthesis Restores Vision in a Rat Model of Degenerative Blindness. *Nat. Mater.*
19 17 **2017**, *16* (6), 681–689. <https://doi.org/10.1038/nmat4874>.
20 18 (79) Ghezzi, D.; Antognazza, M. R.; Maccarone, R.; Bellani, S.; Lanzarini, E.; Martino, N.; Mete, M.; Pertile,
21 19 G.; Bisti, S.; Lanzani, G.; Benfenati, F. A Polymer Optoelectronic Interface Restores Light Sensitivity in
22 20 Blind Rat Retinas. *Nat. Photonics* **2013**, *7* (5), 400–406. <https://doi.org/10.1038/nphoton.2013.34>.
23 21 (80) Tullii, G.; Desii, A.; Bossio, C.; Bellani, S.; Colombo, M.; Martino, N.; Antognazza, M. R.; Lanzani, G.
24 22 Bimodal Functioning of a Mesoporous, Light Sensitive Polymer/Electrolyte Interface. *Org. Electron.*
25 23 **2017**, *46*, 88–98. <https://doi.org/10.1016/j.orgel.2017.04.007>.
26 24 (81) Vaquero, S.; Bossio, C.; Bellani, S.; Martino, N.; Zucchetti, E.; Lanzani, G.; Antognazza, M. R.
27 25 Conjugated Polymers for the Optical Control of the Electrical Activity of Living Cells. *J. Mater. Chem.*
28 26 *B* **2016**, *4* (31), 5272–5283. <https://doi.org/10.1039/C6TB01129B>.
29
30
31
32
33
34
35
36
37
38
39
40
41
42
43
44
45
46
47
48
49
50
51
52
53
54
55
56
57
58
59
60

1
2
3
4
5
6
7
8
9
10
11
12
13
14
15
16
17
18
19
20
21
22
23
24
25
26
27
28
29
30
31
32
33
34
35
36
37
38
39
40
41
42
43
44
45
46
47
48
49
50
51
52
53
54
55
56
57
58
59
60

